Efficient THz generation from low-temperature-grown GaAs photoconductive antennas driven by Yb-doped fiber amplifier at 200 kHz repetition rate

Niloufar Nilforoushan, C. Kidd, Aurélie Fournier, José Palomo, Jérôme Tignon, Sukhdeep Dhillon, Emmanuel Lhuillier, Lianhe Li, A. Giles Davies, E. Linfield, et al.

Efficient THz generation from low-temperature-grown GaAs photoconductive antennas driven by Yb-doped fiber amplifier at 200 kHz repetition rate

N. Nilforoushan,[1] C. Kidd,[2] A. fournier,[1] J. Palomo,[1] J. Tignon,[1] S. Dhillon,[1] E. Lhuillier,[3] Lianhe Li,[2] A. Giles Davies,[2] E. H. Linfield,[2] J. R. Freeman,[2] J. Mangeney,[1] and J. Mangeney[1]

[1)]*Laboratoire de Physique de l'Ecole Normale Supérieure, ENS, Université PSL, CNRS, Sorbonne Université, Université de Paris, Paris, France*

[2)]*School of Electronic and Electrical Engineering, University of Leeds, Woodhouse Lane, Leeds LS9 2JT, United Kingdom*

[3)]*Sorbonne Université, CNRS, Institut des NanoSciences de Paris, 4 place Jussieu, 75005 Paris, France*

(*Electronic mail: Author to whom correspondence should be addressed: juliette.mangeney@phys.ens.fr)

(*Electronic mail: Author to whom correspondence should be addressed: niloufar.nilforoushan@phys.ens.fr)

(Dated: 23 April 2024)

We demonstrate the generation of THz pulses with electric field strength reaching 34 kV/cm from low-temperature-grown GaAs (LT-GaAs) interdigitated photoconductive antennas (PCAs) driven by 1030 nm optical pulses delivered by a commercial ytterbium-doped fiber laser operating at a repetition rate of 200 kHz. By probing the Urbach absorption in LT-GaAs layers, we show that the THz generation mechanism predominantly relies on the photoexcitation of electrons from the valence band to shallow defect states arising from the incorporation of excess As during the growth process. Our THz source opens the route toward nonlinear time-resolved study of low-energy excitations in matter with high signal-to-noise ratios.

Recent years have witnessed significant progress in the generation of high-intensity terahertz (THz) pulses with single- and few-cycle duration. These sources have opened up new avenues for the direct exploration, manipulation, and coherent driving of low-energy excitations and lattice vibrational modes in quantum materials on their intrinsic time scales[1,2]. Particular examples are THz pulses with peak electric fields exceeding several tens of kilovolts per centimeter, which serve as a unique tool for probing nonlinear light-matter interactions, including high-harmonic generation[3–5], optical Stark effect[6,7], and collective excitations of ordered phases such as Higgs bosons in superconducting states[8,9]. The prevailing sources of intense THz pulses are currently driven by femtosecond optical pulses at $\sim$800 nm wavelength, generated by Ti:sapphire amplifiers that operate at low repetition rates (in the kHz range)[10–13]. Nevertheless, many applications necessitate a high signal-to-noise ratio, thereby calling for an increase in the repetition rate of the excitation optical pulse train. Recently, the advent of Yb-doped fiber amplifiers capable of delivering femtosecond pulses centered at 1030 nm and at repetition rates of hundreds of kHz with energies reaching hundreds of μJ has facilitated the realization of intense THz pulses at high repetition rates. Indeed, using Yb-doped fiber amplifiers, mW-level THz pulses at repetition rates $>$100 kHz with peak electric fields exceeding 100 kV/cm by optical rectification[14,15] and of 1 MV/cm peak electric fields by two-color plasma generation[16] have been recently reported.

In the pursuit of compact intense THz sources with a repetition rate of a few hundred kHz[17], photoconductive antennas (PCAs) deserve particular attention as they deliver THz pulses with high spectral amplitudes below 3 THz. Moreover, their ability to be electrically modulated at high frequencies further mitigates noise-related issues in THz spectroscopy and imaging systems. PCAs based on low-temperature-grown (LT) GaAs driven by optical pulses at 800 nm wavelength delivered by Ti:Sapphire amplifiers are widely used for the generation of intense THz pulses at low repetition rate[18–20]. Intensive efforts are devoted to the development of PCAs driven by longer wavelength optical pulses matching those delivered by powerful Yb-doped lasers. To this purpose, lower energy bandgap semiconductors, which associate short carrier lifetimes and high resistivity are being investigated[21–24]. For instance, very broadband THz pulses (up to 70 THz) from Au-implanted germanium-based PCAs excited by 1100 nm optical pulses at 10 MHz repetition rate have recently been reported with moderate peak electric fields of $\sim$0.8 kV/cm[24]. However, the potential of PCAs as sources of intense THz pulses at repetition rates in the hundreds of kHz range remains elusive so far.

In this work, we demonstrate the generation of intense THz pulses with peak electric fields of up to 34 kV/cm at a repetition rate of 200 kHz by large-area interdigitated LT-GaAs PCAs illuminated by 1030 nm wavelength optical pulses delivered by a ytterbium-doped fiber laser. We investigate both wide- and small-gap devices, identify the optical saturation regime, and show that the emitted THz spectra are in the low-frequency part of the THz spectral range, i.e. below $\sim$3 THz.

The 2-μm-thick LT-GaAs layers used in this work as active layers of the PCAs were grown at 290 °C by molecular beam epitaxy and subsequently annealed for 15 min at 550 °C.The PCAs are fabricated by bonding the LT-GaAs layer to an insulating sapphire substrate using benzocyclobutene. The growth process details can be found in Ref.[19]. Sapphire,

with its high level of insulation and coefficient of thermal expansion close to that of GaAs, is an ideal substrate for high-energy optical excitation pulses, as it significantly delays the thermal breakdown of the devices. To prevent destructive interference of THz pulses between adjacent gaps of the PCAs, we remove the LT-GaAs layer in every-other gap instead of masking them. Using this method, we fabricate two interdigitated devices: a small-gap and a wide-gap device. The small-gap device allows for the application of a low bias voltage modulated at a frequency of several tens of kHz, achievable with a standard function generator, while still delivering near-breakdown electric fields across the electrodes[25], which is very promising for achieving a high signal-to-noise ratio. On the other hand, the wide-gap device benefits from an easier fabrication process, and optical saturation effects occur later, as they are less affected by space-charge screen effects[26]. However, large electrode spacing requires a high-voltage power supply, in the kV range, which is known to add electronic noise. The wide-gap device has LT-GaAs gaps of 130 μm, an area of 2 mm×2 mm, and consists of 7 active gaps, while the small-gap device has gaps of 5 μm, an area of 1 mm×3 mm and contains 78 active gaps. Optical microscope images of the LT-GaAs PCA devices are shown in Fig. 1 (a). The electrodes are made up of Ti/Au (15/200 nm) and their width is 50 μm on the wide-gap antenna and 5 μm on the small-gap device.

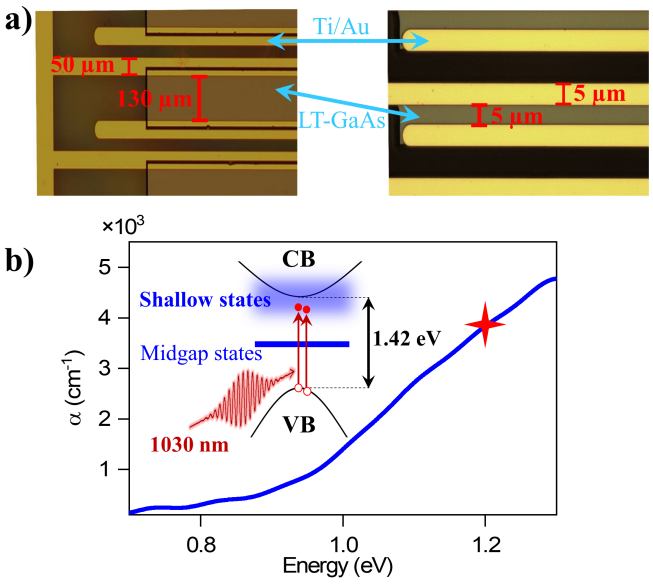

FIG. 1. (a) Optical microscope images of the LT-GaAs PCAs devices studied in this work. The wide- and small-gap devices are displayed on the left- and right-hand side respectively. The LT-GaAs gaps and the Ti/Au electrodes are shown. (b) Absorption coefficient of the LT-GaAs layer as a function of photon energy. The star corresponds to 1030 nm wavelength. The inset shows a schematic diagram of the energy levels in LT-GaAs. Photons with less energy than the bandgap excite electrons from the valence band to shallow-level defect states.

Previous studies have shown that the absorption of LT-GaAs differs considerably from that of semi-insulating GaAs[27], which is zero at 1.2 eV (λ = 1030 nm) due to its larger bandgap energy (1.42 eV). Indeed, the incorporation of excess As in the form of arsenic antisite and arsenic interstitial point defects during the growth at low temperatures induces local potential fluctuations in the LT-GaAs, which result in a quasi-continuum of weakly bound shallow defect states in the vicinity of the conduction band (see Fig 1 (b), inset). These shallow defect states promote the absorption of photons with energy lower than the SI-GaAs bandgap energy, leading to a spectral broadening of the absorption edge referred to as the Urbach absorption tail[28,29]. Subsequent annealing of the LT-GaAs layer results in the precipitation of a large number of point defects in the As clusters, which give rise to mid-gap states acting as effective capture and recombination centers for photoexcited carriers. To gain insight into the Urbach absorption of the LT-GaAs active layer, we measured its absorption spectrum using Fourier transform infrared spectroscopy in transmission geometry. Figure 1 (b) shows the absorption coefficient of LT-GaAs layer from 0.7 to 1.3 eV, revealing a large absorption in this spectral range due to the Urbach tail. The absorption coefficient at 1.2 eV reaches 3 900 cm^{-1}, a value consistent with previous works[27] and which is exploited here to achieve THz emission from LT-GaAs photoconductive antenna driven by optical pulses at λ = 1030 nm.

Next, we investigate the coherent THz radiation emitted from the LT-GaAs PCAs excited by 30-fs-long optical pulses centered at 1030 nm delivered by a Yb-doped fiber laser operating at 200 kHz repetition rate. Our optical setup is explained in detail in Ref.[14]. The PCAs are illuminated by a divergent optical beam, corresponding to a spherical wavefront optical excitation[30], using a 1/2 inch parabolic mirror with an f-number of 2. The optical pulse energy can be tuned up to 45 μJ (9 W). We record the THz pulses generated by the PCA devices in transmission geometry using electro-optic sampling in a $\langle 110 \rangle$-cut ZnTe crystal of a thickness 200 μm. To minimize attenuation and dispersion of the THz pulses in the sapphire substrate, we employ back-side illumination, allowing the optical beam to pass through the substrate before exciting the LT-GaAs active layer. To apply electric fields of several tens of kV/cm (E_{bias}) to the wide-gap PCA, we use a high-voltage DC power supply delivering hundreds of volts. The emitted THz signal is modulated using an optical chopper operating at a frequency of 625 Hz placed on the excitation pump beam. In contrast, we apply electric fields of several tens of kV/cm to the small-gap PCA using a standard waveform generator delivering a few volts square bias, modulated at a frequency of 18 kHz.

Figure 2 (a) depicts the emitted THz waveforms from the wide- and small-gap devices. For these measurements, we illuminate the entire active region of the antenna. The temporal waveforms are asymmetrically bipolar with a first peak resulting from the fast rise of the surge current by the injection of the photocarriers and their subsequent acceleration under the bias field. The rise time from the negative to the positive cycle is about 350 fs. The corresponding amplitude spectra obtained by the fast Fourier transform of

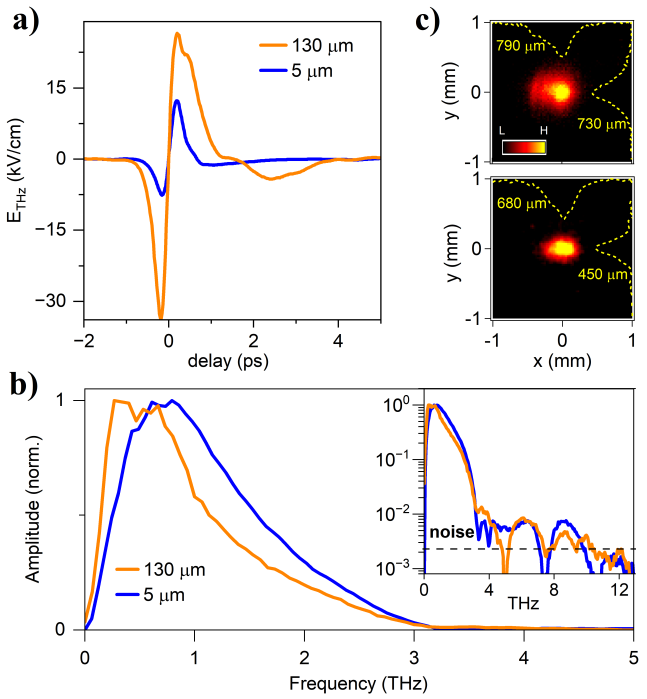

FIG. 2. (a) Time-domain waveforms from the wide-gap emitter biased at 450 V (E_{bias}= 34.6 kV/cm) and small-gap emitter biased at 15 V (E_{bias}= 30 kV/cm), driven by optical pulses with incident fluences of 1.5 mJ.cm^{-2} and 0.4 mJ.cm^{-2}, respectively. (b) The amplitude spectra obtained by the fast Fourier transform of the time-domain waveforms. The inset displays the amplitude spectra on a logarithmic scale. (c) The THz spot images at the focus for the wide-gap (upper) and small-gap (lower) devices. Superimposed are the intensity profiles along the x coordinate (y=0) and y coordinate (x=0).

the waveforms are displayed in Fig. 2 (b). The spectra have a central frequency at ∼0.4 THz and ∼0.7 THz for the wide- and small-gap devices, respectively, with spectral components extending up to 3.2 THz. The higher central frequency of the emitted spectrum for the low-gap device is attributed to faster spatial charge screening effects of the polarizing field when the electrode spacing is reduced[31]. We attribute the high-frequency dips observed in the logarithmic spectra (inset Fig. 2 (b)) to echoes in the time-domain signals. The THz pulse duration is determined by extracting the intensity profile of the Hilbert transform of the THz transient. The wide-gap device exhibits a pulse duration of 487 fs, while the small-gap device has a pulse duration of 458 fs. The signal-to-noise ratio is about 450 (i.e. 53 dB in power) for an integration time of the lock-in amplifier of 500 ms.

The spatial profiles of the THz beams are probed using an uncooled micro-bolometer camera. The two-dimensional spatial distributions in the focal plane of the THz beams, with (x,y) as the coordinate framework, are displayed in Fig. 2 (c) upper for the wide-gap emitter and lower for the small-gap emitter. The waist radius are w_x=395 μm, w_y=365 μm for the wide-gap emitter and w_x=340 μm, w_y=225 μm for the small-gap emitter. We measure the average THz power by replacing the THz camera with a calibrated pyroelectric power meter. The THz average power emitted by the wide-gap device reaches 340 μW, corresponding to a conversion efficiency of 3.9 $\times 10^{-5}$, and that emitted by the small-gap device reaches 22 μW, corresponding to a conversion efficiency of 3.1 $\times 10^{-6}$. From average THz power, THz beam spot size, and electro-optical measurements we estimate a maximum peak electric field of ∼ 34 kV/cm generated by the wide-gap device and of 12.3 kV/cm for the small-gap device, demonstrating THz electric field strengths of a few tens of kV/cm at a repetition rate of 200 kHz. These electric field amplitudes are comparable with those emitted by BNA organic crystals of 29 kV/cm at 540 kHz repetition rate[32], but the latter requires low duty-cycle pump chopping to suppress thermal effects[33] whereas LT-GaAs PCAs can be electrically modulated at high repetition rates. Also, THz electric field strengths of up to 79 kV/cm at 400 kHz repetition rate have been recently reported using lithium niobate crystals but with a lower frequency spectrum[34].

Next, we investigate the dependence of the THz electric field emitted by the LT-GaAs PCAs on bias electric field and optical fluence. The linear growth of the peak-to-peak THz electric field with applied electric field observed in Fig. 3 (a) indicates the absence of any valley scatterings of photogenerated carriers up to 34.6 kV/cm. We emphasize that due to the different active areas of the two devices and the different THz signal modulation techniques, whether electrical or optical depending on the device, the data show the performance of each THz emitting device, but do not provide a quantitative comparison of their efficiency. The maximum voltage that could be applied to each device was limited by the breakdown of air between the narrower gaps where the LT-GaAs material had been removed. We probe the fluence dependence of the THz electric field emitted by the wide-gap device in order to limit the effects of antenna capacitance, which are less important for the wider gap. Figure 3 (b) shows that the THz electric field amplitude increases linearly with the incident optical fluence at low fluences and exhibits a saturation behavior at high fluences. To interpret the observed saturation regime, we derive the peak-to-peak amplitude of the THz electric field, E_{pp}, considering that the local electric field acting on the photoexcited carriers is the sum of the applied electric field and the polarization resulting from the space charge induced by the separation of photoexcited electrons and holes at the end of the optical pulses[35], giving $E_{\rm pp} \propto F_{\rm laser}/(F_{\rm laser}+F_0)$ with $F_0 = \varepsilon h\nu/(q\alpha(1-e^{-\alpha l})\mu\tau_{\rm las})$. ε is the permittivity of the LT-GaAs, l is the thickness of the LT-GaAs layer, α its absorption coefficient at the laser energy, μ the electron mobility in the LT-GaAs layer, $h\nu$ the optical photon energy and $\tau_{\rm las}$ the pulse duration. The excellent agreement between the experimental data and the fit validates our simple analysis and highlights the effective screening of the applied electric field by the space-charge field at high photocarrier density. With ε= 10.9ε_0, l= 2 μm, α= 3900 cm^{-1}, $h\nu$= 1.2 eV and $\tau_{\rm laser}$= 30 fs, we extract the mobility μ = 1800 cm^{2}V^{-1}s^{-1} from the fit corresponding to the mobility of electrons in high concentration in the early

phase after their creation.

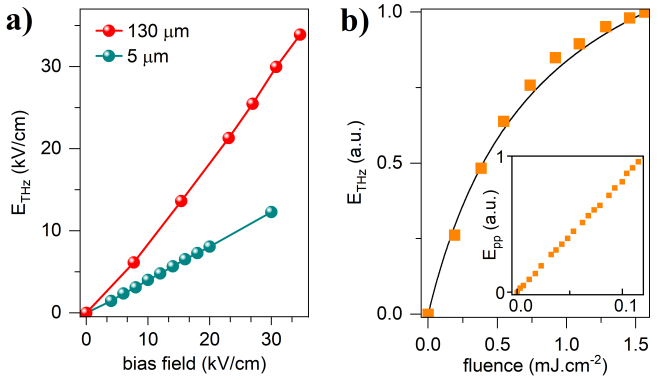

FIG. 3. (a) THz peak-to-peak electric field as a function of bias field for the wide-gap emitter (fluence, 1.5 mJ.cm^{-2}) and small-gap emitter (fluence, 0.4 mJ.cm^{-2}). (b) E_{THz} versus optical excitation fluence incident on the wide-gap device. The solid black line shows the saturation law model. The inset shows the THz electric field growth in the low fluence regime.

The linear rise of the emitted electric field at low optical pump fluences, highlighted in the inset of Fig. 3 (b), provides evidence that two-photon absorption processes do not contribute to the mechanism of THz generation[36,37]. Consequently, the THz generation mechanism solely involves photoexcited electrons from the valence band to the shallow defect states in the vicinity of the conduction band. We assume that the photoelectrons are trapped within the shallow defect states and must escape to the conduction band, by hopping or scattering, to be effectively accelerated by the bias electric field and subsequently radiated THz waves. Consequently, we attribute the limited bandwidth of the emitted THz spectra to the escape time of trapped electrons to the conduction band, which delays electron acceleration by the bias electric field. In other words, the pulse duration no longer limits the THz spectra but it is mainly the time needed for photoelectrons trapped in As defect states to reach the conduction band. This explanation is further supported by a comparison of the THz spectra emitted by the small-gap LT-GaAs PCA when illuminated by optical pulses at a wavelength of 1030 nm and at a wavelength of 800 nm. For the illumination with optical pulses at 800 nm wavelength, we use an experimental set-up based on a Ti:sapphire amplifier[19]. We observe in Fig. 4 (a) that the amplitude spectrum emitted by the PCA excited by optical pulses at 800 nm wavelength extends up to 5.5 THz and is therefore significantly broader than that emitted by the PCA excited by optical pulses at 1030 nm wavelength, while the optical pulse durations are essentially similar (45 fs for optical pulses at 800 nm wavelength). We attribute this enhanced bandwidth to the fact that at the 800 nm wavelength optical pulses excite electrons directly from the valence band to the conduction band resulting in an emission process that is mainly limited by the optical pulse duration rather than the escape time of trapped photocarriers. Furthermore, we compare the THz spectra emitted by the LT-GaAs PCA emitter and by optical rectification in a 1 mm-thick gallium phosphide (GaP) crystal, both excited by optical pulses at a wavelength of 1030 nm, in the same experimental setup. As shown in 4 (b), the THz spectrum emitted by the GaP crystal is broader, confirming that the low-frequency THz spectrum emitted by LT-GaAs PCAs excited at 1030 nm is not limited by the bandwidth of our experiment. Therefore, the THz pulses emitted by LT-GaAs PCAs excited by optical pulses with a wavelength of 1030 nm concentrate their energy in the low-THz frequency range, which is difficult to access using nonlinear crystals.

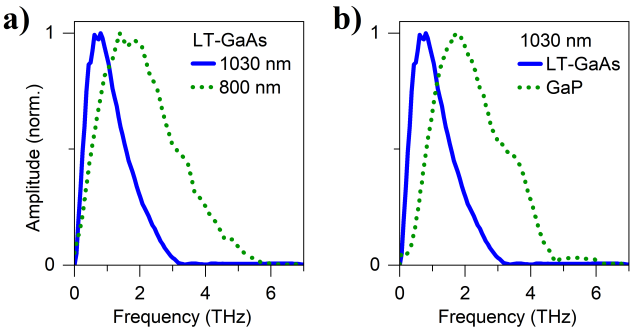

FIG. 4. (a) Amplitude spectra of THz pulses emitted from the LT-GaAs PCA excited by optical pulses at a wavelength of 1030 nm and at a wavelength of 800 nm. (b) Amplitude spectra of THz pulses delivered by a LT-GaAs PCA and a GaP crystal under identical excitation configuration with optical pulses at 1030 nm wavelength.

In conclusion, we have shown the potential of LT-GaAs PCAs excited by optical pulses at 1030 nm wavelength as sources of intense THz pulses at a repetition rate of 200 kHz. We have demonstrated the generation of THz pulses whose spectra lie in the low-frequency part of the THz spectral range (<3 THz) with an electric field strength exceeding 34 kV/cm. Our source fills a critical gap that is challenging to address using optical rectification in nonlinear crystals and paves the way for time-resolved studies of low-energy excitations in matter with a high signal-to-noise ratio. Finally, the absorption efficiency, and potentially bandwidth, of the LT-GaAs PCAs driven at 1030 nm could be improved by optimizing the annealing temperature of the LT-GaAs layer, by adding an anti-reflective coating for 1030 nm, or by adding plasmonic nano-structures to LT-GaAs surface. Increasing the absorption efficiency of LT-GaAs PCAs driven at 1030 nm would allow saturation to be reached with lower fluences thereby allowing larger arrays for the same optical pulse energy and higher fields to be generated.

ACKNOWLEDGMENTS

This project was supported by ERC Consolidator Grant LEON (Grant No. 820133) and EPSRC UK programmes EP/W028921/1 and EP/P021859/1. This work was also sup-

ported by French State Funds managed by the ANR using Grant QuickTera (No. ANR-22-CE09-0018) and STEM2D (No. ANR-19-CE24-0015).

DATA AVAILABILITY STATEMENT

The data that support the findings of this study are available from the corresponding author upon reasonable request.

[1] T. Kampfrath, K. Tanaka, and K. A. Nelson, "Resonant and nonresonant control over matter and light by intense terahertz transients," Nat. Photonics **7**, 680–690 (2013).

[2] X. C. Zhang, A. Shkurinov, and Y. Zhang, "Extreme terahertz science," Nat. Photonics **11**, 16–18 (2017).

[3] H. A. Hafez, S. Kovalev, J.-C. Deinert, Z. Mics, B. Green, N. Awari, M. Chen, S. Germanskiy, U. Lehnert, J. Teichert, Z. Wang, K.-J. Tielrooij, Z. Liu, Z. Chen, A. Narita, K. Müllen, M. Bonn, M. Gensch, and D. Turchinovich, "Extremely efficient terahertz high-harmonic generation in graphene by hot Dirac fermions," Nature **561**, 507–511 (2018).

[4] S. Kovalev, R. M. A. Dantas, S. Germanskiy, J.-C. Deinert, B. Green, I. Ilyakov, N. Awari, M. Chen, M. Bawatna, J. Ling, F. Xiu, P. H. M. van Loosdrecht, P. Surówka, T. Oka, and Z. Wang, "Non-perturbative terahertz high-harmonic generation in the three-dimensional Dirac semimetal Cd_3As_2," Nat. Commun **11**, 2451 (2020).

[5] F. Meng, M. D. Thomson, Q. ul Islam, B. Klug, A. Pashkin, H. Schneider, and H. G. Roskos, "Intracavity third-harmonic generation in Si:B pumped by intense terahertz pulses," Phys. Rev. B **102**, 075205 (2020).

[6] B. C. Pein, W. Chang, H. Y. Hwang, J. Scherer, I. Coropceanu, X. Zhao, X. Zhang, V. Bulović, M. Bawendi, and K. A. Nelson, "Terahertz-Driven Luminescence and Colossal Stark Effect in CdSe–CdS Colloidal Quantum Dots," Nano Lett. **17**, 5375–5380 (2017).

[7] M. Wagner, H. Schneider, D. Stehr, S. Winnerl, A. M. Andrews, S. Schartner, G. Strasser, and M. Helm, "Observation of the intraexciton Autler-Townes effect in GaAs/AlGaAs semiconductor quantum wells," Phys. Rev. Lett. **105**, 167401 (2010).

[8] R. Matsunaga, N. Tsuji, H. Fujita, A. Sugioka, K. Makise, Y. Uzawa, H. Terai, Z. Wang, H. Aoki, and R. Shimano, "Light-induced collective pseudospin precession resonating with Higgs mode in a superconductor," Science **345**, 1145–1149 (2014).

[9] N. Yoshikawa, H. Suganuma, H. Matsuoka, Y. Tanaka, P. Hemme, M. Cazayous, Y. Gallais, M. Nakano, Y. Iwasa, and R. Shimano, "Ultrafast switching to an insulating-like metastable state by amplitudon excitation of a charge density wave," Nat. Phys. **17**, 909–914 (2021).

[10] M. Shalaby, C. Vicario, T. Karunanithi, S. Brahadeeswaran, and C. P. Hauri, "Intense THz source based on BNA organic crystal pumped at conventional Ti:Sapphire wavelength," Opt. Lett. **41**, 1777 (2016).

[11] R. Piccoli, A. Rovere, Y.-G. Jeong, Y. Jia, L. Zanotto, F. Légaré, B. E. Schmidt, R. Morandotti, and L. Razzari, "Extremely broadband terahertz generation via pulse compression of an Ytterbium laser amplifier," Opt. Express **27**, 32659–32665 (2019).

[12] L. Guiramand, J. E. Nkeck, X. Ropagnol, T. Ozaki, and F. Blanchard, "Near-optimal intense and powerful terahertz source by optical rectification in lithium niobate crystal," Photonics Res. **10**, 340 (2022).

[13] T. Seifert, S. Jaiswal, M. Sajadi, G. Jakob, S. Winnerl, M. Wolf, M. Kläui, and T. Kampfrath, "Ultrabroadband single-cycle terahertz pulses with peak fields of 300 kV cm^{-1} from a metallic spintronic emitter," Appl. Phys. Lett. **110**, 252402 (2017).

[14] N. Nilforoushan, T. Apretna, C. Song, T. Boulier, J. Tignon, S. Dhillon, M. Hanna, and J. Mangeney, "Ultra-broadband THz pulses with electric field amplitude exceeding 100 kV/cm at a 200 kHz repetition rate," Opt. Express **30**, 15556–15565 (2022).

[15] P. L. Kramer, M. K. R. Windeler, K. Mecseki, E. G. Champenois, M. C. Hoffmann, and F. Tavella, "Enabling high repetition rate nonlinear THz science with a kilowatt-class sub-100 fs laser source," Opt. Express **28**, 16951–16967 (2020).

[16] J. Buldt, H. Stark, M. Müller, C. Grebing, C. Jauregui, and J. Limpert, "Gas-plasma-based generation of broadband terahertz radiation with 640 mW average power," Opt. Lett. **46**, 5256–5259 (2021).

[17] I. E. Ilyakov, B. V. Shishkin, V. L. Malevich, D. S. Ponomarev, R. R. Galiev, A. Y. Pavlov, A. E. Yachmenev, S. P. Kovalev, M. Chen, R. A. Akhmedzhanov, and R. A. Khabibullin, "Efficient optical-to-terahertz conversion in large-area InGaAs photo-Dember emitters with increased indium content," Opt. Lett. **46**, 3360 (2021).

[18] A. Singh, J. Li, A. Pashkin, R. Rana, S. Winnerl, M. Helm, and H. Schneider, "High-field THz pulses from a GaAs photoconductive emitter for nonlinear THz studies," Opt. Express **29**, 19920–19927 (2021).

[19] D. R. Bacon, T. B. Gill, M. Rosamond, A. D. Burnett, A. Dunn, L. Li, E. H. Linfield, A. G. Davies, P. Dean, and J. R. Freeman, "Photoconductive arrays on insulating substrates for high-field terahertz generation," Opt. Express **28**, 17219–17231 (2020).

[20] D. You, R. R. Jones, P. H. Bucksbaum, and D. R. Dykaar, "Generation of high-power sub-single-cycle 500-fs electromagnetic pulses," Opt. Lett. **18**, 290–292 (1993).

[21] M. S. Kong, J. S. Kim, S. P. Han, N. Kim, K. Moon, K. H. Park, and M. Y. Jeon, "Terahertz radiation using log-spiral-based low-temperature-grown InGaAs photoconductive antenna pumped by mode-locked Yb-doped fiber laser," Opt. Express **24**, 7037–7045 (2016).

[22] R. J. B. Dietz, B. Globisch, M. Gerhard, A. Velauthapillai, D. Stanze, H. Roehle, M. Koch, T. Göbel, and M. Schell, "64 μW pulsed terahertz emission from growth optimized InGaAs/InAlAs heterostructures with separated photoconductive and trapping regions," Appl. Phys. Lett. **103**, 061103 (2013).

[23] A. Urbanowicz, V. Pačebutas, A. Geižutis, S. Stanionytė, and A. Krotkus, "Terahertz time-domain-spectroscopy system based on 1.55 μm fiber laser and photoconductive antennas from dilute bismides," AIP Advances **6**, 025218 (2016).

[24] A. Singh, A. Pashkin, S. Winnerl, M. Welsch, C. Beckh, P. Sulzer, A. Leitenstorfer, M. Helm, and H. Schneider, "Up to 70 THz bandwidth from an implanted Ge photoconductive antenna excited by a femtosecond Er:fibre laser," Light sci. appl. **9**, 30 (2020).

[25] A. Dreyhaupt, S. Winnerl, T. Dekorsy, and M. Helm, "High-intensity terahertz radiation from a microstructured large-area photoconductor," Appl. Phys. Lett. **86**, 121114 (2005).

[26] X. Ropagnol, X. Chai, S. M. Raeis-Zadeh, S. Safavi-Naeini, M. Kirouac-Turmel, M. Bouvier, C.-Y. Côté, M. Reid, M. A. Gauthier, and T. Ozaki, "Influence of gap size on intense thz generation from znse interdigitated large aperture photoconductive antennas," IEEE J. Quantum Electron. **23**, 1–8 (2017).

[27] S. U. Dankowski, D. Streb, M. Ruff, P. Kiesel, M. Kneissl, B. Knüpfer, G. H. Döhler, U. D. Keil, C. B. Sørenson, and A. K. Verma, "Above band gap absorption spectra of the arsenic antisite defect in low temperature grown GaAs and AlGaAs," Appl. Phys. Lett. **68**, 37–39 (1996).

[28] F. Urbach, "The Long-Wavelength Edge of Photographic Sensitivity and of the Electronic Absorption of Solids," Phys. Rev. **92**, 1324–1324 (1953).

[29] D. Webber, X. Liu, M. Dobrowolska, J. K. Furdyna, and K. C. Hall, "Control of the Urbach band tail and interband dephasing time with post-growth annealing in low-temperature-grown GaAs," AIP Advances **8**, 045121 (2018).

[30] M. Baillergeau, K. Maussang, T. Nirrengarten, J. Palomo, L. H. Li, E. H. Linfield, A. G. Davies, S. Dhillon, J. Tignon, and J. Mangeney, "Diffraction-limited ultrabroadband terahertz spectroscopy," Sci. Rep. **6**, 24811 (2016).

[31] J. Made, N. Jukam, D. Oustinov, M. Rosticher, R. Rungsawang, J. Tignon, and S. Dhillon, "Frequency tunable terahertz interdigitated photoconductive antennas," Electron. Lett. **46**, 611 – 613 (2010).

[32] S. Mansourzadeh, T. Vogel, A. Omar, M. Shalaby, M. Cinchetti, and C. J. Saraceno, "Broadband, high power THz source at 540 kHz using organic crystal BNA," APL Photonics **8**, 011301 (2023).

[33] Z. B. Zaccardi, I. C. Tangen, G. A. Valdivia-Berroeta, C. B. Bahr, K. C. Kenney, C. Rader, M. J. Lutz, B. P. Hunter, D. J. Michaelis, and J. A. Johnson, "Enabling high-power, broadband THz generation with 800-nm pump wavelength," Opt. Express **29**, 38084–38094 (2021).

[34] C. Millon, S. Houver, and C. J. Saraceno, "400 kHz repetition rate THz-TDS with 24 mW of average power driven by a compact industrial Yb-laser," Opt. Express **31**, 7922–7932 (2023).

[35] J. Mangeney, N. Chimot, L. Meignien, N. Zerounian, P. Crozat, K. Blary, J. Lampin, and P. Mounaix, "Emission characteristics of ion-irradiated $In_{0.53}Ga_{0.47}As$ based photoconductive antennas excited at 1.55 μm," Opt.

Express **15**, 8943–8950 (2007).

[36] J.-M. Rämer, F. Ospald, G. von Freymann, and R. Beigang, "Generation and detection of terahertz radiation up to 4.5 THz by low-temperature grown GaAs photoconductive antennas excited at 1560 nm," Appl. Phys. Lett. **103**, 021119 (2013).

[37] M. Tani, K.-S. Lee, and X.-C. Zhang, "Detection of terahertz radiation with low-temperature-grown GaAs-based photoconductive antenna using 1.55 μm probe," Appl. Phys. Lett. **77**, 1396–1398 (2000).